Taylor & Francis
Taylor & Francis Group

A GLOBAL NO$_X$ SUBMODEL FOR PULVERIZED COAL FLAMES AT ELEVATED PRESSURES

GUI-SU LIU
STEPHEN NIKSA[*]

Niksa Energy Associates, Belmont, California, USA

This study formulates a global NO$_X$ submodel for deployment in CFD simulations from a database on flames of three diverse coals at pressures to 3.0 MPa for broad ranges of stoichiometric ratio (S.R.). A new reaction scheme was formulated from a sensitivity analysis of simulations based on detailed reaction mechanisms for all tests. It shares many elements in common with commercial submodels, yet it correctly predicts that (1) less coal-N is converted into NO; and (2) HCN persists to higher S.R. for progressively higher pressures. Explicit dependences on O$_2$ concentrations are responsible for the first feature, because the variations in O$_2$ concentrations mimic the ways that the oxyhydroxyl radical pool shrinks at progressively higher pressures, which shifts HCN conversion toward N$_2$ production. The second feature was depicted by resolving the intermediate products of HCN decomposition in the global scheme. Discrepancies surfaced when the new submodel was applied to different coals without re-adjusting rate parameters, which probably reflects a generic limitation of global NO$_X$ production submodels for coal combustion.

Keywords: burner simulations, CFD, NO$_X$ emissions, pressure, pulverized coal

INTRODUCTION

Across the globe developers of coal-fired power generators face impera-
tives to raise conversion efficiencies to compete better with other fuels,
especially where CO_2 emissions are being reduced. A multitude of
advanced process concepts are under development, as surveyed recently
by Beer (2000). All have one thing in common: Primary conversion of the
coal feed at elevated pressure. Major blocks in the technical foundation
supporting development of pressurized coal conversion technology are
already in place. The impact of elevated pressure on the rates and yields
of the coal conversion kinetics are clearly evident in extensive databases
for devolatilization and char oxidation (Niksa et al., 2003a). The database
on char gasification needs to be expanded further (Liu and Niksa, 2004),
but only because so many operating conditions and char characteristics
are important. Notwithstanding these essential elements of pressurized
pulverized coal (p.c.) flames, we have not found any characterization work
in the English literature on the structures of actual p.c. flames at elevated
pressures.

     This study finalizes the interpretation of a database on flames of
three diverse coals at pressures to 3.0 MPa for broad ranges of stoichio-
metric ratio (S.R.). The first level of analysis used CFD simulations to
determine flame structures and assign detailed operating conditions for
all tests (Liu and Niksa, 2005b). The second level specified equivalent
reactor networks for the flowfields, then interpreted the post-flame gas
compositions with detailed reaction mechanisms (Niksa and Liu,
2005). In this, the third and final level, we first identify the dominant
fuel-N conversion channels from the simulations based on detailed
mechanisms, then formulate and fully specify a global NO_X submodel
for deployment in CFD simulations. Once the submodel has been vali-
dated against the detailed chemistry simulations, it is used to assess
the impact of pressure on NO_X production for a realistic fuel injector
configuration.

DATABASE

The test facility simulated the thermal and chemical environments in the
primary zone of a pulverized coal flame without the complications of
two-phase turbulent mixing. As explained elsewhere in detail (Liu and
Niksa, 2005), the coal burner was a vertically mounted, cylindrical flow
reactor that imposed uniform radial heat fluxes comparable to those in

utility burners. An intense external radiant field stabilized the reaction fronts so that the burner could operate with any inlet O_2 level, including none at all in cases that determined the distributions of secondary pyrolysis products. As suspensions moved along the flow tube, they were heated at rates approaching $10^{4}°C/s$ to the onset temperature for primary devolatilization, released their volatiles, and burned. At any particular operating condition, O_2 depletion eventually "quenched" the chemistry at an intermediate stage determined by the proportions of coal and O_2 at the inlet. Inlet O_2 levels were progressively increased in successive cases to move the process chemistry through oxidative volatiles pyrolysis, volatiles combustion, soot combustion, and char oxidation.

The database comprises six test series that characterized Pit. #8 high volatile (hv) bituminous at 1.0, 2.0, and 3.0 MPa; Ill. #6 hv bituminous at 1.0 and 2.0 MPa; and PRB subbituminous at 1.0 MPa only. The coal properties appear in Table 1. Note the extremely high sulfur contents of the Ill. #6 and Pit. #8 samples and the high ash content of the Ill. #6, which are characteristic of raw, as-mined samples. These coals were obtained from the Penn State Database, then aerodynamically classified. The tested samples were a mixture of two sieve sizes, 75 to 90 μm and 90 to 105 μm, so the mean size was about 90 μm. Each test series contains from seven to ten individual tests with progressively higher inlet O_2 levels, hence, S.R. values. The suspension loadings were decreased from 4.7 wt.% at 1.0 MPa, to 2.3–2.5% at 2.0 MPa, to 1.55% at 3.0 MPa; in other words, coal feedrates were essentially the same at all test pressures. Inlet O_2 mass fractions were regulated at the higher pressures to impose similar ranges of S.R. values in all test series. The maximum S.R. values were near-unity with Pit. #8; 1.77 with Ill. #6; and 1.27 with PRB.

Table 1. Coal properties

Coal name	Proximate analysis, ar wt.%				Ultimate analysis, daf wt.%				
	M	Ash	VM	FC	C	H	O*	N	S
Pit. #8	0.7	12.3	37.9	49.1	80.8	5.4	5.8	1.7	6.3
Ill. #6	0.2	17.3	35.8	46.7	74.1	5.5	8.2	1.4	10.8
PRB	0.1	5.0	39.4	55.5	73.7	5.6	19.0	1.1	0.6

*Assigned by difference.

FLAME STRUCTURES

One could reasonably have expected that the upward flowing, sheathed cylindrical p.c. suspensions in the burner closely approached the idealized structures of planar, 1D flames. But this simple view is contradicted by the coexistence of O_2, CO, and H_2 in the products of every test that had O_2 at the burner inlet. It was also superceded by the complex flame structures in the CFD simulations, which are largely determined by the accumulation of particles in the turbulent boundary layer on the flow tube wall (Liu and Niksa, 2005). At the inlet, particles were only injected into the central core of the flow; an annular sheath flow surrounded the entrained suspension to help prevent particles from colliding with the tube wall. Nevertheless, the particles acquired significant radial velocity components due to the turbulence. Once the particles moved into the boundary layer, they were unlikely to escape back into the core flow, so particles accumulated in the boundary layer and depleted the suspension loading in the core.

As the flow moved through the tube, a flame front propagated from the wall toward the flow axis, driven by convective heat transfer from the wall and by the heat release from combustion of gaseous volatiles and soot. This flame marks the penetration of the thermal layer toward the centerline, but does not indicate the major fuel consumption patterns, because major portions of the combustibles burn both within the volatiles flame and behind it. Within the core, residual gaseous fuels, soot, and char may eventually reach their ignition threshold and burn in a premixed mode. Residual CO, H_2, and char burn in the near-wall region after the volatiles flame has propagated deeper into the core as long as O_2 is available.

Flames were classified as either "closed" or "open" depending on whether or not the volatiles flame propagated into a single parabolic surface through the centerline in the available residence time. Flame closure was mainly determined by pressure and S.R. Inlet conditions that formed closed flames at a lower test pressure eventually sustained open flames at progressively higher pressures. The impact of decreasing S.R. is qualitatively similar. For lower S.R., the volatiles flame in the near-wall region released less heat, because its burning rate was slower at the lower O_2 level. The slower heat release in the near-wall region slowed the convection rate into the core, which delayed ignition, and the lower O_2 level diminished the heat release after the core finally ignited. These joint effects lowered core gas temperatures.

SIMULATIONS WITH DETAILED CHEMISTRY

Equivalent Reactor Networks

Our method to specify equivalent reactor networks from CFD simulations, called ChemNet® CFD post-processing, has been applied to similar lab-scale flames at atmospheric pressure (Niksa and Liu, 2002a) and also to much larger flames (Niksa and Liu, 2003; Niksa et al., 2003b). The reactor networks for the pressurized p.c. flames were developed in three stages. First, conventional CFD simulations generated flow and thermal fields and particle trajectories for each test. Second, conserved scalar fields from the CFD simulations were analyzed to subdivide the flow into regions that sustained distinctive chemistry. Each region was characterized with 1D average profiles of temperature and residence time, a residence time distribution, and an O_2 entrainment history. This information completely specifies an equivalent reactor network for the entire flow. Third, the process chemistry was simulated with detailed reaction mechanisms across all elements in the reactor network.

The CSTR network for the baseline case of Pit. #8 at 1.0 MPa with an S.R. of 0.953 appears in Figure 1. The networks for all other flames have similar branches and feedstreams but appreciably different quantitative specifications. Based on the accumulation of particles near the flow tube wall, the flowfield was subdivided into two cylindrical regions: a near-wall region and a core region. Each core and boundary layer is subdivided into three axial zones. An attachment zone (not indicated in Figure 1) simply conveys fuel components deeper into the burner because this entrance region is too cool to sustain any chemistry. The
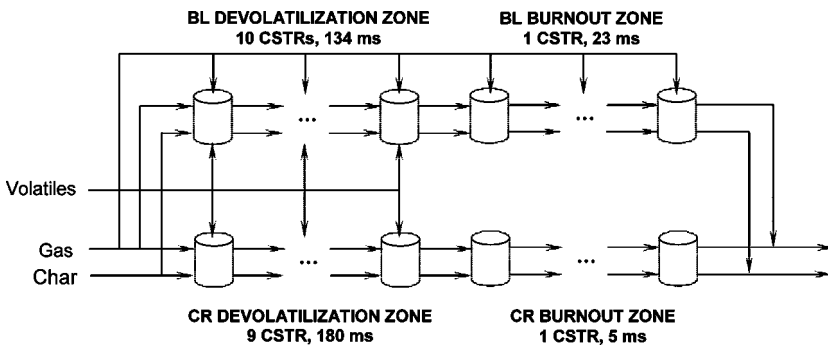

Figure 1. Equivalent reactor network for Pit. #8 flame at 1.0 MPa and a S.R. of 0.953.

devolatilization zone covers the upstream portion of the reacting flow where volatiles are being released from fuel particles and burned with the entrained O_2. Devolatilization is represented as a series of discrete additions of volatiles to the CSTR-series for both flows, based on the corresponding yield increments and gas compositions in stand-alone devolatilization simulations. Burnout zones appear downstream, where gas chemistry is minimal but char continues to burn.

Due to their dissimilar suspension loadings and heat fluxes, the core and near-wall regions have different thermal histories. According to the CFD simulation, the mean gas temperature in the boundary layer increased from 800°C to a maximum of 1550°C at 105 ms, then cooled to about 1000°C at the tube exit. The gas temperature history for the core was much cooler over almost the entire reactor length, but ultimately increased to 1530°C at the tube exit. The volatiles flame for this baseline case is closed. In tests in which the flame does not close across the centerline, the gas temperature history for the core remains much cooler even at the tube exit.

Separate particle temperature histories for the near-wall region and core were evaluated from the particle trajectories in the CFD simulation to assign a thermal history for the devolatilization simulations. Although the same radiation flux is imposed onto all particles, coal particles in the boundary layer were heated at 7600°C/s, versus 5500°C/s in the core, simply because the gas temperature in the boundary layer is hotter. The population of particle trajectories also determined the fuel split into the near-wall layer from the core. From 75 to 90% of the coal was diverted into the near-wall region, where the upper end of this range pertains to cases at 1.0 MPa. From 75 to 80% was diverted at the higher test pressures.

Core fluid is entrained into the CSTR-series for the near-wall region. The O_2 entrainment histories were expressed as fractions of the O_2 flowrate at the core that penetrated through the boundary of the wall layer, based on fluid element tracking. The entrainment history for the near-wall layer simulations was discretized to assign entrainment increments for each reactor in the CSTR-series.

Detailed Reaction Mechanisms

FLASHCHAIN®, the devolatilization submodel, determined the complete distribution of primary volatiles from the fuel's proximate and

ultimate analyses (Niksa, 1995). A mechanism for secondary volatiles pyrolysis transformed the primary volatiles into soot, CO, CO_2, H_2O, H_2, and HCN, which are the fuels injected into the CSTR network. FLASHCHAIN® also predicted the yield and elemental composition of char, and was combined with a swelling factor correlation and a correlation for the initial carbon density in char to specify all the necessary input for a char oxidation simulation.

The reaction mechanism for the homogeneous combustion and N-species conversion was formulated by Glarborg et al. (1998), and contains 444 elementary reactions among 66 species, including all relevant radicals and N-species. All rate parameters were assigned independently by the primary developers, so there are no adjustable parameters in the submodel for gas phase chemistry.

Our soot chemistry submodel combines the mechanism of Pedersen et al. (1998) with a four-step reaction sequence for oxidation by O_2 that determines the same overall oxidation rate law as Nagle-Strickland-Constable kinetics. The rate constants were initially specified to fit the soot oxidation rates reported by Park and Appleton (1973) for temperatures to $1800°C$ and O_2 concentrations to 25%. This collection of elementary reactions cleanly couples to the homogeneous reaction mechanism within the CHEMKIN/SURFACE CHEMKIN framework.

Char burning rates were evaluated with CBK/E, a version of the Carbon Burnout Kinetics (CBK) Model expressly developed for applications at elevated pressures (Hurt and Calo, 2001; Niksa et al., 2003a). This mechanism accounts for thermal annealing, ash encapsulation (of low-rank chars), and a transition to chemical kinetic control, and depicts the impact of variations in gas temperature, O_2 level, and char particle size within useful quantitative tolerances. However, it is not yet possible to specify the initial char reactivity within useful tolerances from the standard coal properties. We must calibrate this value for each fuel sample with a single extent of char conversion or some other suitable index on combustion efficiency. The submodel for char-N conversion is subject to a similar calibration requirement (with NO emissions), compounded by its simplistic mechanistic premise; viz., that a fixed fraction of char-N is converted into NO at the overall burning rate throughout all stages of char oxidation.

The only fuel-dependent adjustable parameters were the initial char oxidation reactivity and the fraction of char-N converted into NO. In our simulations, once these parameters were specified for the baseline

case with a particular coal sample, they remained the same throughout all other simulation conditions with this fuel. The fraction of char-N converted into NO was 0.2 for both Pit. #8 and PRB, and 0.7 for Ill. #6.

NO$_X$ Production

Near-burner flame zone chemistry, especially fuel-N conversion, is largely determined by the products of secondary volatiles pyrolysis. Primary devolatilization products are unstable at flame temperatures, so tars are very rapidly converted into soot plus substantial amounts of CO, H$_2$, and HCN, while chain hydrocarbons are reduced to CH$_4$ and C$_2$H$_2$. Well over half the primary volatiles from Pit. #8 was converted into soot, while over 40% was condensed into soot with Ill. #6. With PRB, less than 20% was converted, which is still not negligible. Clearly, soot plays a major role in the chemistry of near-burner flame zones, because the time scale for its subsequent oxidation is much longer than for the gaseous fuel compounds.

Hydrocarbon gases were eliminated first as progressively more O$_2$ was added to the burner. As S.R. was increased at fixed pressure, the measured weight loss due to devolatilization and char oxidation increased monotonically, as did the CO$_2$ yield. The soot yield diminished as it was burned away in tests with the higher S.R. The CO yield passed through a maximum at a S.R. near 0.5. The H$_2$ yield decreased monotonically.

The most important impact of pressure is seen in the nitrogen speciation versus S.R. in Figure 2. All the N-species concentrations are expressed as percentages of the coal-N. From left-to-right, the three upper panels show the impact of pressure increases with Pit. #8, and the first two lower panels show the pressure dependence with Ill. #6. Note the doubled scale for PRB at 1.0 MPa in the lower right corner. With all coals at all pressures, the N-speciation shifts, as expected, from a predominance of HCN at the lowest S.R., toward minor amounts of NH$_3$ at intermediate S.R., toward rapid NO production at the highest S.R. For all cases, N$_2$ presumably becomes the major fixed-N species for all S.R. above 0.5. But two features for S.R. above 0.7 are striking and unanticipated: First, the conversions of coal-N into NO at all pressures are much lower than from the same fuels in similar flames at atmospheric pressure.
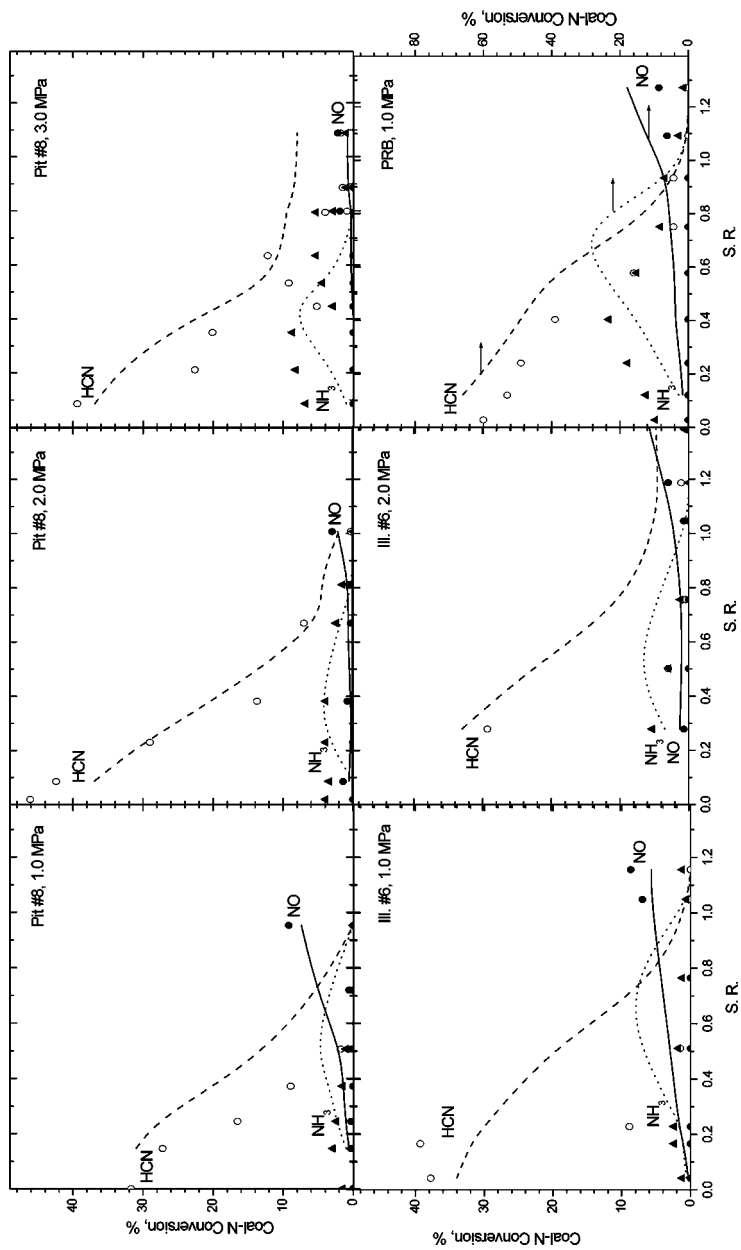
Figure 2. Nitrogen speciation vs. S.R. for (top row) Pit. #8 at 1.0 (left), 2.0 (center), and 3.0 (right); and for (bottom row) Ill. #6 at 1.0 (left) and 2.0 (center) MPa. The lower right panel shows N-speciation for PRB at 1.0 MPa on an expanded scale.

For example, in tests in the radiant burner at 0.1 MPa, subbituminous and Pit. #8 coals converted 21 and 16%, respectively, of their coal-N into NO at S.R. just over unity (Niksa and Liu, 2002b). The comparable conversions at 1.0 MPa for both coals are well under 10%. More importantly, coal-N conversion clearly diminishes for progressively higher pressures with Pit. #8 and Ill. #6. With Pit. #8 it fell from 9.2 to 3.0 to 2.2% as pressure was increased from 1.0 to 2.0 to 3.0 MPa; with Ill. #6 the conversions fell from 8.7 to 5.3% for pressures of 1.0 and 2.0, respectively. The second striking feature in Figure 2 is that HCN persists at S.R. values approaching unity at the highest test pressures. This persistence is stronger at 3.0 MPa than at 2.0 MPa with Pit. #8.

In the predictions for cases with Pit. #8, the coal-N conversion to HCN is over-predicted by the detailed reaction mechanisms through the entire S.R. range, but is qualitatively correct throughout. The ultimate NO conversion is only slightly over-predicted, at 7.4%, vs. a measured value of 5.2%. Ammonia is predicted and observed to be a minor intermediate, although the predicted maximum value at a S.R. of about 0.5 is not apparent in the measured values. Predicted coal-N conversions are more accurate at both elevated pressures. At 2.0 MPa, the conversion to HCN is accurately predicted across the entire range of S.R. The NO is also accurately predicted throughout, with a discrepancy of less than 1.0% for the run at the highest S.R. The predicted maximum in the NH_3 levels is more pronounced than the trend in the data, but most predictions are within experimental uncertainty. At 3.0 MPa, the predicted HCN levels are generally within experimental uncertainty, except that the persistence of HCN for S.R. values over unity cannot be validated due to substantial scatter in the data for these conditions. Again, the maximum in the NH_3 levels is more pronounced in the predictions than in the data. Most important, the analysis predicts less conversion to NO over the full range of S.R. for progressively higher pressures, and the persistence of HCN at higher S.R. values.

For Ill. #6, the coal-N conversion to HCN at the lowest and the highest S.R. is predicted within experimental uncertainty for both 1.0 and 2.0 MPa. Unfortunately, measured HCN levels for intermediate S.R. values were either not recorded or are badly scattered, so a quantitative evaluation is not possible. Ammonia levels are over-predicted throughout, and exhibit maxima that are not apparent in the data. Nevertheless, the predicted NO levels are accurate across the full range of S.R., and again indicate that coal-N conversion to NO diminishes for

progressively higher pressures. For PRB, the coal-N conversion to HCN is slightly over-predicted for S.R. values below 0.85, but exhibits the correct qualitative form. The predicted NH_3 levels are qualitatively correct but shifted toward higher S.R. by 0.30. For the first time, the NO predictions are only qualitatively correct because the predicted NO level is double the measured value at the highest S.R.

GLOBAL NO_X PRODUCTION SUBMODEL FOR PRESSURIZED P.C. FLAMES

Since the mid-1980s, CFD simulations of coal-fired utility furnaces have been used to troubleshoot operational problems, forecast emissions, and expedite design changes such as retrofitting with low-NO_X burners and overfire air injection (Niksa, 1996). Simulations are now routinely tuned-in to measured exhaust NO_X emissions for any furnace firing con-figuration with low-NO_X or circular burners. The best case studies satisfy evaluations with measurements from various power stations firing an assortment of coals (Visona and Stanmore, 1998).

To accommodate the severe restrictions on the number of species in CFD simulations of coal-fired furnaces, such calculations utilize radi-cally simplified process schemes called "global NO_X production sub-models." Such submodels are applied to converged fields for all major species concentrations, temperature, and gas velocity, as a means to decouple the trace species chemistry from the primary variables. This section presents a new NO_X submodel for pressurized p.c. flames, follow-ing a performance evaluation of a current submodel with the pressurized flame database.

The Reference NO_X Submodel

Our reference NO_X submodel is distributed with v.6.1 of FLUENT. It represents thermal, prompt, and fuel NO_X formation as well as NO_X consumption due to hydrocarbon reburning. Since all the tests used an Ar carrier gas, there was no thermal or prompt NO formed, and these mechanisms were omitted from all succeeding simulations. Only the pro-cesses for fuel-derived NO were retained, as seen in Figure 3. Devolati-lization partitions coal-N into HCN and char-N, based on an input parameter assignment. Char-N is released into the gas phase at the char oxidation rate as either HCN or NO; no char-N is directly converted into
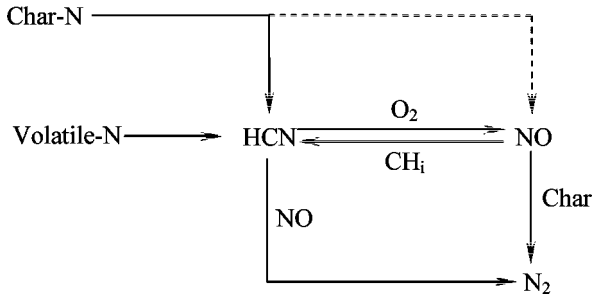
Figure 3. Diagram of coal-N reaction pathways in the v.6.1 FLUENT NO_X submodel.

N_2. De Soete's two-step process describes HCN conversion, as follows:

$$HCN + O_2 \rightarrow NO + \cdots \tag{1}$$

$$HCN + NO \rightarrow N_2 + \cdots \tag{2}$$

Default parameter values for the preexponential factors, activation energies and reaction orders for these two reactions were reported by De Soete (1975).

The heterogeneous reaction that reduces NO on char in Figure 3 is based on the model of Song and co-workers (1981), which requires a BET char surface area whose default value in FLUENT is $2.5 \times 10^4 \, m^2/kg$. The NO reburning step eliminates NO via hydrocarbon chemistry at temperatures from 1327 to 1827°C. However, NO and hydrocarbons never coexisted in either the data or the detailed chemistry simulations (Niksa and Liu, 2004), so NO reburning was deemed to be negligible.

We repeated our original CFD simulations, which accurately depicted all major species concentrations (Liu and Niksa, 2004b), with the v.6.1 NO_X submodel to obtain the two sets of predictions in Figure 4. One set is based on the default parameter assignments, and a second is a "best fit" that reflects unconstrained parameter adjustments. Although the default NO_X submodel qualitatively depicts the impact of S.R. on HCN and NO levels, there are huge quantitative discrepancies for all test conditions. The HCN levels are over-predicted for all S.R., and HCN is predicted to persist for S.R. values near-unity, at odds with the data. This flaw in the predictions worsens for progressively higher pressures, so that 40% of coal-N was predicted to appear as HCN for the highest S.R. at 3.0 MPa, but none was measured. Moreover, the
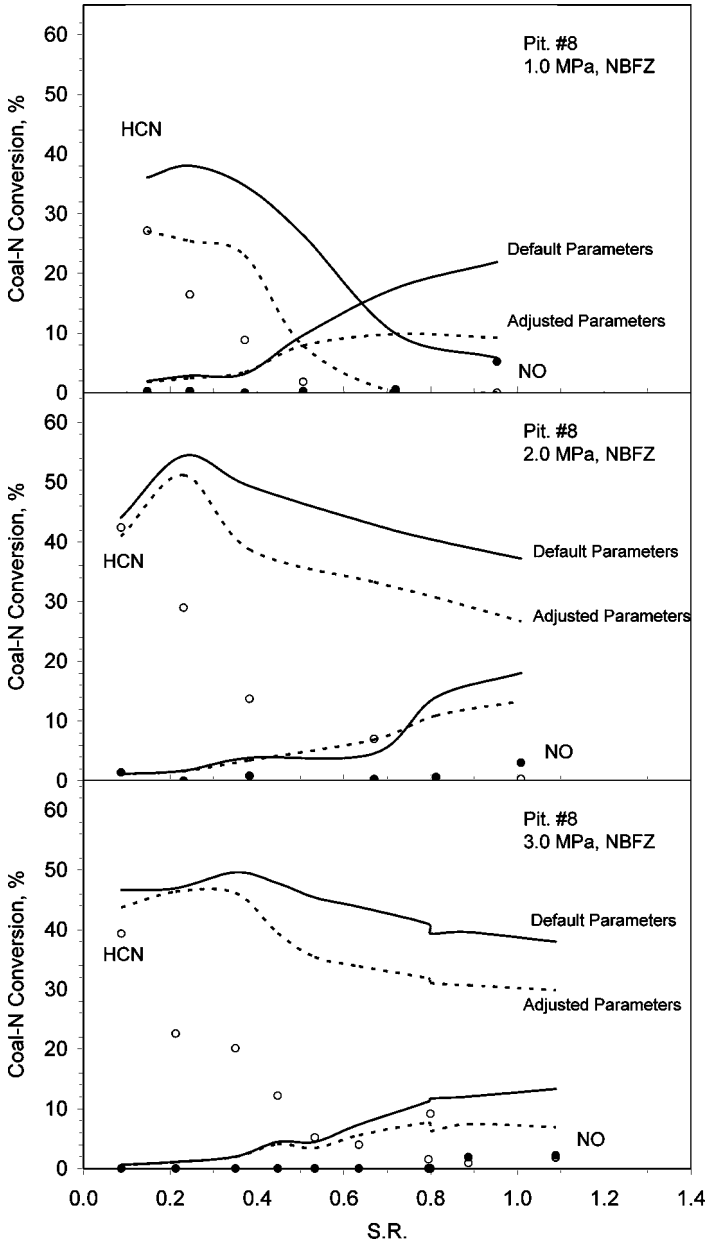
Figure 4. Evaluation of predictions from v.6.1 FLUENT NO$_X$ submodel with default parameters (solid curves) and with adjusted parameters (dashed curves) for Pit. #8 at 1.0 (upper), 2.0 (middle) and 3.0 MPa (lower) with the measured HCN ($\circ$) and NO ($\bullet$) levels.

conversion of coal-N into NO is predicted to approach 25% at 1.0 MPa, which is a typical value for atmospheric combustion for this coal type (Niksa and Liu, 2002b). Whereas the NO predictions diminish for progressively higher pressures, they are always 3 to 5 times higher than the measured values. All char-N was converted into NO in the simulations, which may be partly responsible for the over-prediction of NO. However, if the only other option of converting all char-N into HCN was applied, then the HCN predictions would be even worse. All these flaws are evident in the evaluation with both Ill. #6 data sets. Surprisingly, the default submodel only slightly over-predicts HCN levels over the entire range of S.R. for the PRB test series, but the extent of the over-predictions in the NO levels is even worse than for both other coals.

To rectify these flaws, the default pre-exponential factors were first increased by a factor of 10 to see if the earlier flaws could be attributed to default parameters, but not the proposed reaction scheme. Subsequent attempts to use even faster rates yielded essentially the same predictions, because NO and HCN were no longer simultaneously present in the same regions, so the impact of Eq. (2) reached a saturation limit. The predicted HCN and NO levels from the v.6.1 FLUENT NO_X submodel were improved by adjusting rate parameters, but serious flaws associated with the proposed reaction scheme persisted throughout the test domain. In particular, the conversion of coal-N into NO was always seriously over-predicted, whereas HCN was predicted to persist at much higher S.R. values than recorded in the tests.

A New Global NO_X Submodel

A group of the detailed chemistry simulations was selected for sensitivity analysis to identify the major channels for fuel-N conversion, and to evaluate specific reaction rates and intermediate species concentrations. All such cases were for Pit. #8 in order to cover the widest possible ranges of pressure, temperature, and S.R. The rate-of-production analysis indicated that HCN was converted into NO and N_2 mostly through two parallel paths involving NCO and NH_i. CN, HOCN, HNCO only appeared as intermediates in these two major paths. N_2 and NO were the major ultimate products of HCN-conversion, whose relative yields depended on the gas environment.
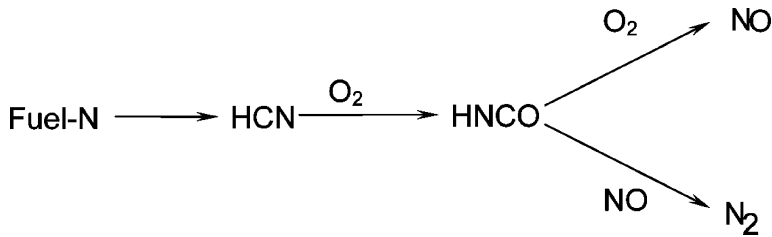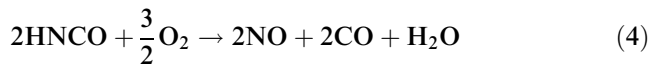
Figure 5. Global scheme for HCN conversion into NO and N_2 developed from sensitivity analysis of the detailed chemistry simulations for tests with Pit. #8.

N_2O and NO_2 were minor products for the test conditions, so these species and their associated reactions were omitted from the global mechanism.

The global scheme in Figure 5 represents the most important channels in the elementary reaction mechanism with the following three steps:

$$HCN + \frac{1}{2}O_2 \rightarrow HNCO \tag{3}$$

$$2HNCO + \frac{3}{2}O_2 \rightarrow 2NO + 2CO + H_2O \tag{4}$$

$$2HNCO + NO \rightarrow \frac{3}{2}N_2 + 2CO + H_2O \tag{5}$$

The scheme is the same as the v.6.1 FLUENT NO_X submodel except for the addition of two features: (1) The intermediate decomposition products of HCN, HCNO and amines, are explicitly represented as pseudo-HNCO; and (2) The additional concentration dependences on O_2 and NO are also explicit in each of the three steps. The first addition is required to depict the high levels of residual HCN in the tests at moderate temperatures even for S.R. values greater than unity. For progressively higher pressures at moderate temperatures, the oxyhydroxyl radical pool (O, OH, and H) shrinks, which decelerates the rate of HCN conversion into HNCO and amines. The second addition is needed to depict less NO production for progressively higher pressures in the NBFZ tests. While the oxyhydroxyl radical pool shrinks at elevated pressures, the conversion of HNCO shifts toward N_2 production, so the predicted NO levels are lower, consistent with the data.

Table 2. Rate parameters in the new global NO_X submodel

Reaction	A, s^{-1}	E, kcal/mol	O_2 order
R_3	6.0×10^2	0.625	1
R_4	9.0×10^2	1.421	1
R_5	2.0×10^6	1.174	—

For consistency with the detailed chemistry simulations, a fixed fraction of char-N was converted into NO in the global submodel (and specified as 0.2 for Pit. #8 and PRB, and 0.7 for Ill. #6). NO reduction on soot was omitted from the global submodel, because it made a small contribution to N-species conversion in the detailed chemistry simulations.

Reactions 3 and 4 each contain unspecified frequency factors, activation energies and orders with respect to O_2. Reaction 5 contains an unspecified frequency factor and activation energy. These parameters were specified to fit the Pit. #8 data sets, as indicated in Table 2. The specified rate parameters are very small, which is not surprising considering the multitude of elementary reactions lumped into each process in the global scheme.

As seen in Figure 6, the HCN predictions from the new global submodel are in better agreement than the detailed chemistry predictions for Pit. #8 at 1.0 MPa, whereas the NO predictions are the same. For 2.0 and 3.0 MPa, all the predictions for both species are comparable, except that the NO predictions from the global submodel are slightly higher at the highest S.R. values. Note that the new global submodel predicts that HCN persists in the flue gas for S.R. values greater than unity. Hence, the new global submodel correctly depicts the impact of pressure on NO production for the highest S.R. cases.

For Ill. #6, HCN levels from the global submodel for 1.0 and 2.0 MPa were more accurate than the detailed chemistry predictions, particularly for intermediate S.R. values. The predicted NO levels were accurate throughout the test series at 1.0 MPa, but were almost double the measured values for 2.0 MPa. Similarly, for PRB at 1.0 MPa, predicted HCN levels were as accurate as the detailed chemistry predictions, but the NO prediction was about 3 times larger than the measured value for the run with the highest S.R. (Niksa and Liu, 2004).
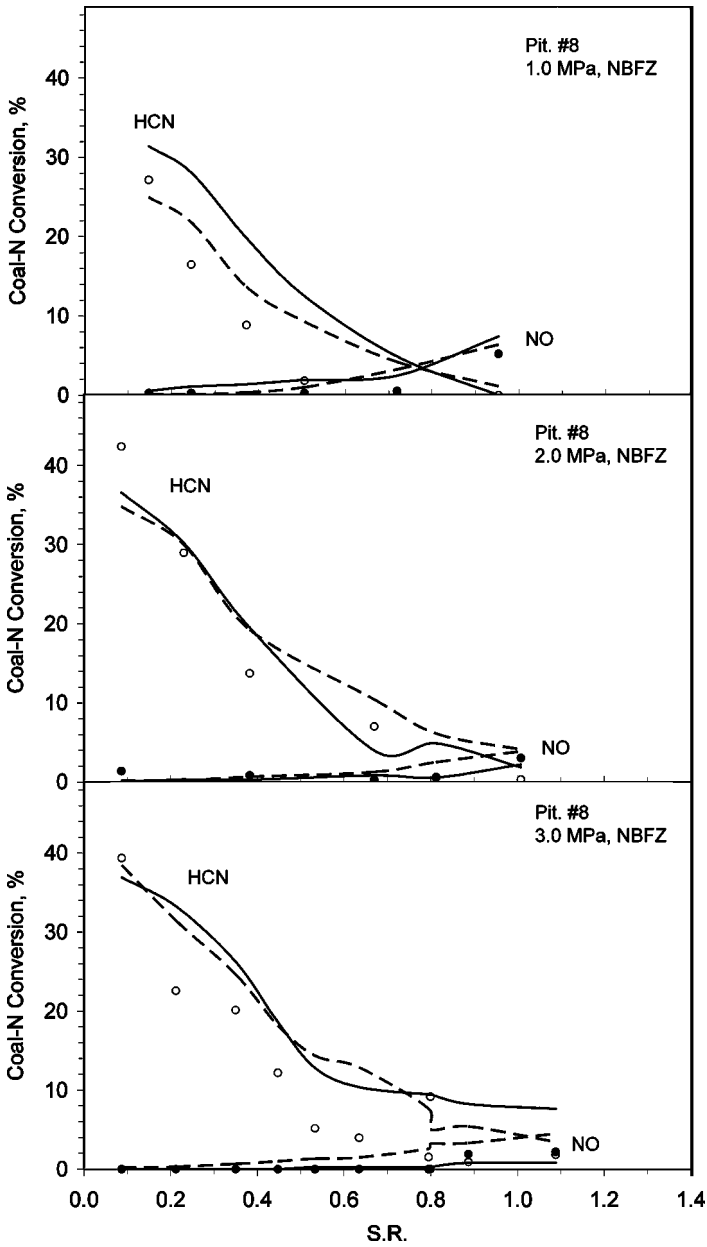
Figure 6. Evaluation of predictions from the new NO_X submodel (dashed curves) for Pit. #8 at 1.0 (upper), 2.0 (middle) and 3.0 MPa (lower) with the measured HCN (○) and NO (●) levels and the predictions from the detailed chemistry simulations (solid curves).

Evaluations for Near-Injector Flame Zones

The complex flow and particle dispersion patterns in the tests admit the possibility that the apparent impact of pressure on NO production could be attributable to variations in other operating conditions for progressively higher pressures (Niksa and Liu, 2005). In particular, for progressively higher pressures, the turbulence intensified; gas temperatures became significantly cooler; and the extents of char burnout diminished. All these factors affect the NO emissions in the post-flame products, and obscure the impact of pressure, per se. In order to focus on the pressure effect, the near-burner region around a typical fuel injector was simulated as follows: The injector was fired with a standard utility grind of Pit. #8 with a 55 μm mean size and an overall S.R. of 1.15. The suspension loading was 3% at all pressures. Particles were forced to remain in the core of the flow by switching off the stochastic dispersion submodel in FLUENT so that the O_2 in the sheath flow was gradually entrained into the core. This is the typical situation immediately downstream of the fuel injectors for tangential firing. Nearly identical temperature histories for gases were imposed at all pressures. These CFD simulations were post-processed to specify reactor networks in order to predict the NO and HCN levels with full chemistry.

The detailed reaction mechanisms predicted very low conversion of coal-N into NO at typical flame temperatures for elevated pressures. For a uniform extent of char burnout of 64%, the fractional coal-N conversion progressively decreased from 6.3 to 3.0 to 1.4% as pressure was increased from 1.0 to 2.0 and 3.0 MPa. For an S.R. of 1.15, no coal-N was converted to HCN at 1.0 and 3.0 MPa, whereas only 1.2% was converted at 2.0 MPa.

These values are compared with predictions from the v.6.1 FLUENT NO_X submodel and the new NO_X submodel in Figure 7. The predicted conversion of coal-N into NO from the FLUENT NO_X submodel is approximately 35% at all three pressures, which is several times larger than that predicted with full chemistry. The predicted HCN levels are comparable with full chemistry at 1.0 and 3.0 MPa, but the prediction for 2.0 MPa is poor. The new NO_X submodel also over-predicts HCN and NO emissions, but by much smaller amounts. It also correctly depicts the impact of pressure on NO, whereby NO emissions decrease for progressively higher pressures. But the quantitative impact is much weaker than seen in the predictions for full chemistry. HCN is predicted
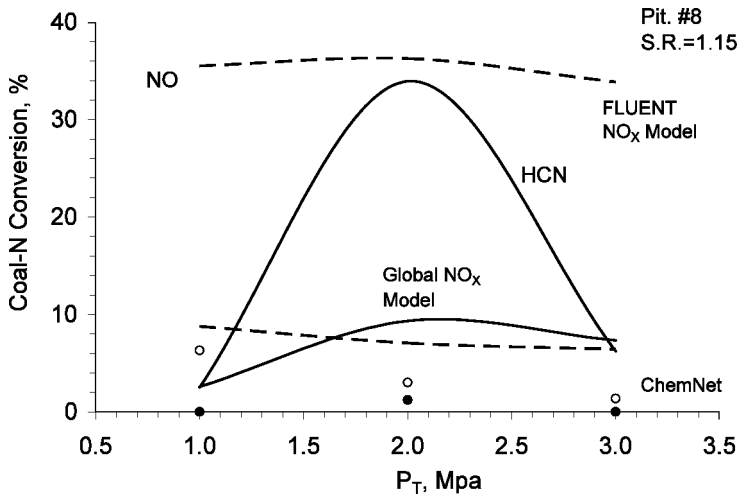
Figure 7. Predictions based on detailed chemistry for HCN (●) and NO (○) compared with predicted HCN (solid line) and NO (dashed line) from the v.6.1 FLUENT NO_X submodel and the new NO_X submodel.

to persist in the flue gas at all pressures, clearly at odds with the full chemistry predictions. The predicted conversion of coal-N into HCN is 2.6, 9.3, and 7.3% at 1.0, 2.0, and 3.0 MPa, respectively.

DISCUSSION

The new NO_X submodel shares many elements in common with the v.6.1 FLUENT NO_X submodel, yet its performance is markedly better. The v.6.1 FLUENT submodel could not interpret the pressurized flame database within useful quantitative tolerances even when applied to CFD simulations that had been fit to predict all the major reaction products, and even when the NO_X submodel parameters were freely adjusted. Predicted NO emissions were much too high, because the submodel overestimates the conversion of coal-N into NO. The new NO_X submodel quantitatively depicted the most important trends in NO emissions with Pit. #8 over the full pressure range from 1.0 to 3.0 MPa. In particular, for progressively higher pressure, (1) less coal-N is converted into NO; and (2) HCN persists to higher S.R. Explicit dependences on O_2 concentrations in the global scheme are responsible for the first advantage,

because the variations in O_2 concentrations mimic the ways that the oxy-hydroxyl radical pool shrinks at progressively higher pressures, which shifts HCN conversion toward N_2 production. The second benefit was obtained by resolving the intermediate products of HCN decomposition in the global scheme. The satisfactory extrapolation from the moderate temperatures in the tests to practical flame temperatures represents a major hurdle that has been sustained.

Discrepancies surfaced when the new submodel was applied to different coals without re-adjusting rate parameters, which probably reflects a generic limitation of global NO_X production submodels for coal combustion. The scheme could be expanded to better represent the coal quality impacts, but only when additional data on several more coals is available to determine the rate parameters. In the interim, the predicted NO levels can be regarded as conservatively high estimates at the highest pressures in the domain, but the predicted HCN levels should be ignored whenever flue gases are strongly oxidizing.

REFERENCES

Beer, J.M. (2000) Combustion technology developments in power generation in response to environmental challenges. *Prog. Energy Combust. Sci.*, **26**(4–6), 301.

De Soete, C.G. (1975) Overall reaction rates of NO and N_2 formation from fuel nitrogen. *Proc. Combus. Inst.*, **15**, 1093.

Glarborg, P., Alzueta, M.U., Dam-Johansen, K., and Miller, J.A. (1998) Kinetic modeling of hydrocarbon/nitric oxide interactions in a flow reactor. *Combust. Flame*, **115**, 1.

Hurt, R.H. and Calo, J.M. (2001) Semi-global intrinsic kinetics for char combustion modeling. *Combust. Flame*, **125**, 1138.

Liu, G.-S. and Niksa, S. (2004) Coal conversion submodels for design applications at elevated pressures. Part II. Coal gasification. *Prog. Energy Combust. Sci.*, **30**(6), 697.

Liu, G.-S. and Niksa, S. (2005) Pulverized coal flame structures at elevated pressures. Part 1. Detailed operating conditions. *Fuel*, **84**(12/13), 1563.

Niksa, S. (1995) Predicting the devolatilization behavior of any coal from its ultimate analysis. *Combust. Flame*, **100**, 384.

Niksa, S. (1996) Coal Combustor Modeling. No. 31, *IEA Perspectives Series*, IEA Coal Research, London.

Niksa, S. and Liu, G.-S. (2002a) Incorporating detailed reaction mechanisms into simulations of coal-nitrogen conversion in p.f. flames. *Fuel*, **81**, 2371.

Niksa, S. and Liu, G.-S. (2002b) Detailed reaction mechanisms for coal-nitrogen conversion in p.f. flames. *Proc. Combust. Inst.*, **29**, 2259.

Niksa, S. and Liu, G.-S. (2003) Advanced CFD Post-Processing for P. F. Flame Structure and Emissions. The 28th International Technical Conference on Coal Utilization and Fuel Systems, March 10–13, 2003, Clearwater, Florida.

Niksa, S. and Liu, G.-S. (2005) Pulverized coal flame structures at elevated pressures. Part 2. Interpreting NO_X production with detailed reaction mechanisms. *Fuel*, **84**(12/13), 1575.

Niksa, S., Liu, G.-S., and Hurt, H. (2003a) Coal conversion submodels for design applications at elevated pressures. Part I. Coal devolatilization and char oxidation. *Prog. Energy Combust. Sci.*, **29**(5), 425.

Niksa, S., Liu, G.-S., Bush, P.V., and Boylan, D.M. (2003b) Predicting the Emissions from Biomass Cofiring. The 28th International Technical Conference on Coal Utilization and Fuel Systems, March 10–13, 2003, Clearwater, Florida.

Park, C. and Appleton, J.P. (1973) Shock-tube measurements of soot oxidation rates. *Combust. Flame*, **20**, 369.

Pedersen, L.S., Glarborg, P., and Dam-Johansen, K. (1998) A reduced reaction scheme for volatile nitrogen conversion in coal combustion. *Combust. Sci. Technol.*, **131**, 193–223.

Song, Y.H., Beer, J.M., and Sarofim, A.E. (1981) Reduction of nitric oxide by coal char at temperatures of 1250–1750 K. *Combust. Sci. Technol.*, **25**, 237.

Visona, S.P. and Stanmore, B.R. (1998) Modeling NO formation in a swirling pulverized coal flame. *Chem. Engr. Sci.*, **53**(11), 2013.